The first wave of T lymphopoiesis in zebrafish arises from aorta endothelium independent of hematopoietic stem cells

Ye Tian,[1] Jin Xu,[1] Shachuan Feng,[1] Sicong He,[2] Shizheng Zhao,[1] Lu Zhu,[1] Wan Jin,[1] Yimei Dai,[1] Lingfei Luo,[3] Jianan Y. Qu,[2] and Zilong Wen[1,4]

[1]Division of Life Science, State Key Laboratory of Molecular Neuroscience and Center of Systems Biology and Human Health and [2]Center of Systems Biology and Human Health, Department of Electronic and Computer Engineering, Hong Kong University of Science and Technology, Clear Water Bay, Kowloon, Hong Kong, P.R. China
[3]Key Laboratory of Freshwater Fish Reproduction and Development, Ministry of Education, Laboratory of Molecular Developmental Biology, School of Life Sciences, Southwest University, Beibei, Chongqing, P.R. China
[4]Shenzhen Key Laboratory for Neuronal Structural Biology, Biomedical Research Institute, Shenzhen Peking University-The Hong Kong University of Science and Technology Medical Center, Guangdong, Shenzhen, P.R. China

T lymphocytes are key cellular components of the adaptive immune system and play a central role in cell-mediated immunity in vertebrates. Despite their heterogeneities, it is believed that all different types of T lymphocytes are generated exclusively via the differentiation of hematopoietic stem cells (HSCs). Using temporal–spatial resolved fate-mapping analysis and time-lapse imaging, here we show that the ventral endothelium in the zebrafish aorta–gonad–mesonephros and posterior blood island, the hematopoietic tissues previously known to generate HSCs and erythromyeloid progenitors, respectively, gives rise to a transient wave of T lymphopoiesis independent of HSCs. This HSC-independent T lymphopoiesis occurs early and generates predominantly CD4 $T_{\alpha\beta}$ cells in the larval but not juvenile and adult stages, whereas HSC-dependent T lymphopoiesis emerges late and produces various subtypes of T lymphocytes continuously from the larval stage to adulthood. Our study unveils the existence, origin, and ontogeny of HSC-independent T lymphopoiesis in vivo and reveals the complexity of the endothelial-hematopoietic transition of the aorta.

INTRODUCTION

Hematopoiesis is a complicated process and consists of multiple waves of development arising from different sources. In mice, the first or primitive wave of hematopoiesis occurs on embryonic day (E) 7 in the yolk sac (YS) and gives rise to embryonic erythrocytes, megakaryocytes, and macrophages (Palis et al., 1999; Palis and Yoder, 2001). The second or intermediate wave of hematopoiesis also arises from the YS on ~E8 and generates erythromyeloid progenitors (EMPs) capable of differentiating into erythroid and myeloid cells (Frame et al., 2013). The third or definitive wave of hematopoiesis emerges on about E10.5 from the aorta–gonad–mesonephros (AGM) and produces hematopoietic stem cells (HSCs; Müller et al., 1994; Medvinsky and Dzierzak, 1996). The AGM-born nascent HSCs subsequently migrate to the fetal liver and finally home to the bone marrow, where they undergo proliferation and differentiation and give rise to all blood lineages during fetal life and adulthood respectively (Müller et al., 1994; Medvinsky and Dzierzak, 1996).

T lymphocytes, or T cells, are key components of the adaptive immune system and play a central role in cell-

mediated immunity (Pancer and Cooper, 2006). On the basis of the expression of T cell receptors, they are classified into two major classes, αβ and γδ T cells, and each class can be further divided into several subclasses with distinct biological functions (Owen et al., 2013; Buchholz et al., 2016). Despite their heterogeneities, it is generally believed that all mature T cells are generated exclusively via the differentiation of HSCs. This conclusion is based mainly on the findings that T cells in adult mice are continuously replenished by the precursors derived from HSCs and that the para-aortic splanchnopleura, which forms the AGM at a later stage, isolated from mouse embryos is able to give rise to T cells in in vitro culture assay and transplantation analysis, whereas the YS fails to do so (Cumano et al., 1996, 2001; Yokota et al., 2006). However, several later studies challenged this view (Nishikawa et al., 1998; Yoshimoto et al., 2012; Böiers et al., 2013). In these studies, the authors have shown that the YS dissected from E9–E9.5 embryos can generate T cells when co-cultured with OP9–DL1 stromal cells in vitro or transplanted into immunodeficient mice, suggesting that the YS could serve as a source for T lymphopoiesis under these artificial conditions. Consistent with this notion, a recent lineage tracing study by Beaudin et al. (2016) identified a Flk2-positive (Flk2+) he-

Check for updates

matopoietic population capable of giving rise to innate-like T lymphocytes when co-cultured with OP9–DL1 stromal cells in vitro or transplanted into recipient mice. Surprisingly, in vivo, the Flk2^{+} hematopoietic precursors are only present in the YS, AGM, and fetal liver during embryonic and fetal stages but are completely absent in adulthood (Boyer et al., 2011; Beaudin et al., 2016), suggesting that it is unlikely that they belong to conventional HSCs. All these findings support the notion that HSC-independent T lymphopoiesis may exist in mice. However, what remains elusive, despite in vitro and cell transplantation studies, is whether HSC-independent T lymphopoiesis indeed exists in vivo and, if so, where it arises and what biological function it plays.

Similarly to mammals, zebrafish experience successive waves of hematopoiesis and produce analogous mature blood cell types (Jing and Zon, 2011; Stachura and Traver, 2011; Sood and Liu, 2012; Jagannathan-Bogdan and Zon, 2013). In zebrafish, primitive hematopoiesis initiates at ∼11 h postfertilization (hpf) in the rostral blood island (RBI) and the posterior lateral mesoderm, and it produces myeloid cells and embryonic erythrocytes, respectively. The definitive wave of hematopoiesis emerges at around 26–28 hpf in the ventral wall of dorsal aorta (DA), a tissue equivalent to the mammalian AGM (the ventral wall of DA is referred as to the AGM hereafter). The AMG-born definitive wave of hematopoiesis generates HSCs, which subsequently migrate to the caudal hematopoietic tissue and finally reside in the kidney, the adult hematopoietic organ in zebrafish. Likewise, a transient intermediate wave of hematopoiesis is also identified to arise from the posterior blood island (PBI) at 24–30 hpf and gives rise to hematopoietic precursors analogous to the mammalian EMPs (Bertrand et al., 2007). Moreover, zebrafish, like mammals, produce multiple classes of T cells (including αβ and γδ T lymphocytes), which also mature in the thymus (Haire et al., 2000; Schorpp et al., 2006; Meeker et al., 2010; Seelye et al., 2016). Thus, the zebrafish serves as an alternative vertebrate model for exploring the ontogeny of different waves of T lymphopoiesis.

In this study, we use a temporal–spatial resolved cell labeling method to investigate the ontogeny of T lymphocytes in zebrafish in vivo. We demonstrate that zebrafish produce two successive waves of T lymphopoiesis from the ventral endothelium of the aorta: an early HSC-independent T lymphopoiesis generating predominantly CD4 $T_{αβ}$ cells during the larval stage and a late HSC-dependent T lymphopoiesis capable of giving rise to various types of T cells from the larval stage to adulthood.

RESULTS

The PBI in situ generates a transient wave of T lymphopoiesis independent of HSCs

To explore the ontogeny of T lymphocytes in zebrafish, we generated a reporter line Tg(lck:loxP-DsRedx-loxP-GFP) in which loxP-DsRedx-loxP-GFP cassette was placed under the T lymphocyte–specific lck promoter (Langenau et al., 2004). This reporter line was outcrossed with the heat shock–

inducible Tg(hsp70:mCherry-T2a-CreER[T2]) fish, and the resulting double-transgenic line Tg(hsp70:mCherry-T2a-CreER[T2];lck:loxP-DsRedx-loxP-GFP) was used for fate-mapping analysis using the infrared-mediated temporal–spatial resolved cell labeling we developed previously (Xu et al., 2015; Fig. 1 A). In this fate-mapping analysis, the temporal–spatial restricted cell labeling is achieved by the induction and activation of CreER via infrared laser irradiation followed by 4-hydroxytamoxifen treatment. Because the loxP-DsRedx-loxP-GFP reporter cassette is under control of the T lymphocyte-specific lck promoter, only T cells derived from the labeled precursors are marked by GFP. The RBI and AGM regions of Tg(hsp70:mCherry-T2a-CreER[T2];lck:loxP-DsRedx-loxP-GFP) embryos were irradiated (RBI, three spots; AGM, four spots) at 14–16 hpf and 26–28 hpf respectively, while the PBI region was irradiated (two spots) at 22 hpf before the AGM-derived hematopoietic stem/progenitor cells colonize this region (Murayama et al., 2006; Jin et al., 2007, 2009; Fig. 1 B). The infrared-irradiated embryos survived to desired stages, and the contribution of each of these regions to T cells was determined by the presence of the GFP^{+} cells in the thymus and other tissues. As expected, in the AGM-irradiated fish, abundant GFP^{+} cells with small and round lymphocytic shape were found in the thymus from 5 d postfertilization (dpf) onward (Fig. 1, C and D). These GFP^{+} cells were restricted exclusively in the thymus during early stages (Fig. S1 A) and continuously present in the thymus, kidney, spleen, and other tissues (such as skin) in juvenile and adulthood (Fig. 1 C and Fig. S1, C and D). In contrast, GFP^{+} cells were completely absent in the RBI-irradiated fish (Fig. 1, C and D; and Fig. S1, C and D). These findings are consistent with the notion that the AGM produces HSCs and the RBI gives rise to only myeloid lineage cells. To our surprise, a significant number of GFP^{+} cells were found to colonize the thymus in the PBI-irradiated fish at 5 dpf (Fig. 1, C and D; and Fig. S1 A). These GFP^{+} cells in the thymus are indeed T lymphocytes as they express T cell–specific marker lck and exhibit lymphocytic cell morphology similar to those derived from the AGM (Fig. 1 C and Fig. S1 A). Strikingly, unlike the AGM-irradiated fish, in which T cells were continuously generated from larval stage to adulthood as shown by the presence of GFP^{+} cells in the thymus of larvae, juvenile and adult fish (Fig. 1 C and Fig. S1, C and D), GFP^{+} T cells in the PBI-irradiated fish were dramatically reduced when they reached juvenile stage and were completely absent by 40 dpf (Fig. 1 C and Fig. S1, B–D). These data suggest that the PBI generates a transient wave of T cells independent of HSCs. To further support this argument, we repeated the fate-mapping analysis with another transgenic line Tg(hsp70:mCherry-T2a-CreER[T2];ubi:loxP-GFP-loxP-mCherry), in which all cell types are marked by GFP and switch to mCherry upon exposure to infrared irradiation and 4-hydroxytamoxifen treatment. Results showed that the AGM-irradiated fish contained mCherry^{+} cells in the pools of hematopoietic stem/precursor cells, lymphoid lineage, and myeloid lineage

3348

Distinct waves of T lymphopoiesis in zebrafish | Tian et al.
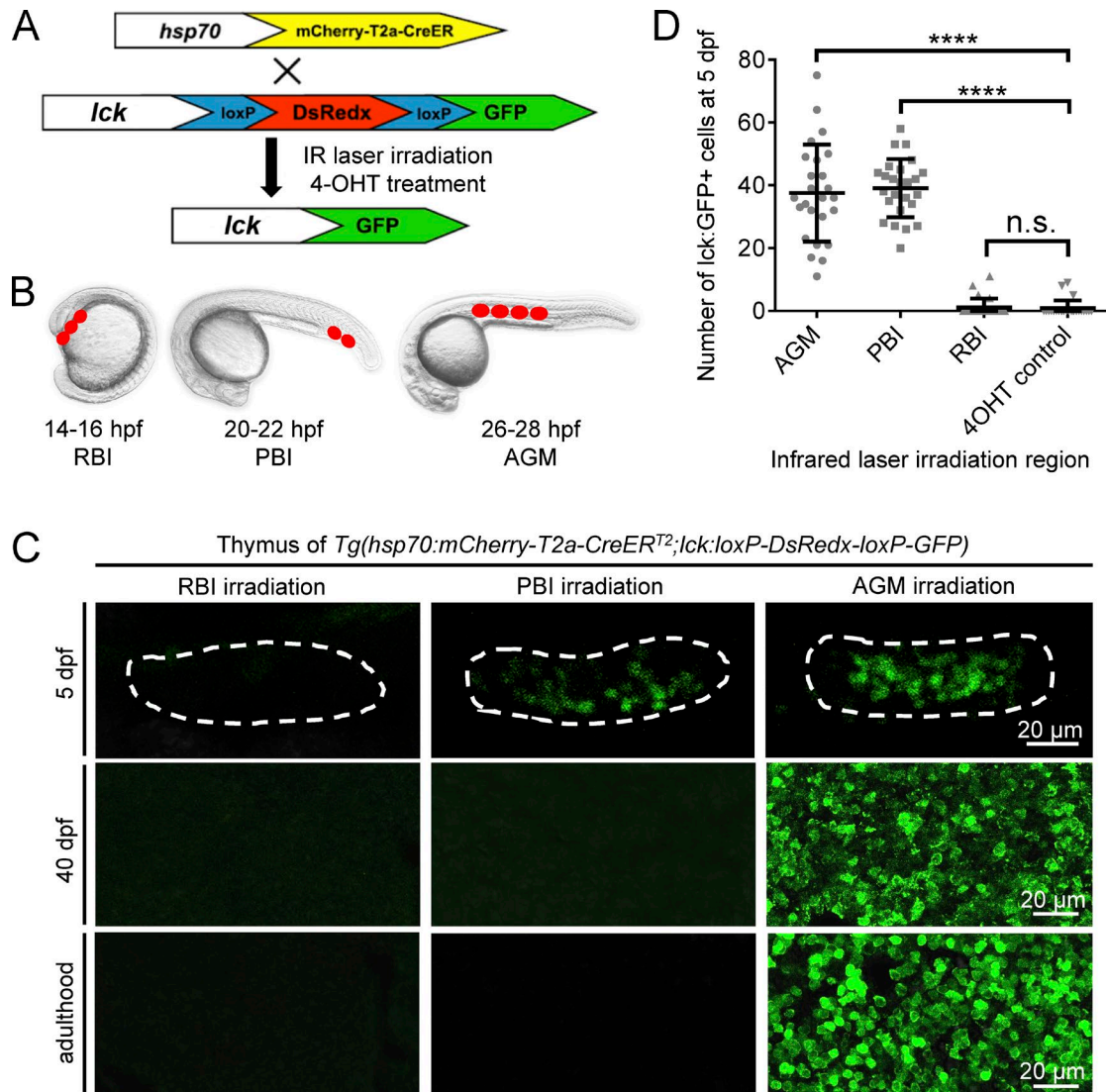
Figure 1. **A transient wave of T cells is in situ generated from the PBI.** (A and B) Outline of the infrared-mediated temporal–spatial cell labeling strategy. The T cell reporter *Tg(lck:loxP-DsRedx-loxP-GFP)* fish are outcrossed with *Tg(hsp70:mCherry-T2a-CreER^T2)* line. The double-transgenic embryos are heat-shocked at restricted regions by infrared (IR) laser irradiation to induce temporal–spatial restricted expression of CreER. After 4-hydroxytamoxifen (4-OHT) treatment, CreER-mediated loxP recombination will remove *DsRedx*, resulting in GFP expression. The RBI region is irradiated at 14–16 hpf with three spots, the PBI region is irradiated at 20–22 hpf with two spots, and the AGM region is irradiated at 26–28 hpf with four spots. The target regions are indicated by red dots, and each dot represents one heat shock spot. (C) Images of *lck*:GFP⁺ cells in the thymus of the RBI-, PBI-, and AGM-irradiated fish at 5 dpf, 40 dpf, and adulthood. Dashed lines depict the thymus of 5-dpf embryos. The signals in the thymus of 5-dpf embryos are captured directly by fluorescent microscope, whereas the signals in the thymus of 40-dpf juveniles and adult fish are imaged after anti-GFP staining of the cryosection. (D) Quantification of *lck*:GFP⁺ cells in the thymus of 5-dpf embryos. AGM (*n* = 25), PBI (*n* = 25), and RBI (*n* = 25) represent embryos that are irradiated by IR and treated with 4-OHT, whereas 4-OHT control (*n* = 25) are embryos treated with 4-OHT only. Data are represented as mean ± SD. Unpaired, two-tailed *t* test was performed to determine significance. ****, P < 0.0001. See also Figs. S1, S2, and S3.

in the adult spleen and kidney, whereas mCherry⁺ cells were completely absent in the PBI-irradiated adult fish, despite the presence of abundant mCherry⁺ cells in the thymus at 5 dpf (Fig. S2), indicating that the PBI does not generate HSCs with long-term multilineage potential. Collectively, these findings demonstrate that in addition to generating EMPs (Bertrand et al., 2007; Fig. S3), the PBI region in situ generates a transient wave of T lymphocytes independent of HSCs.

PBI–derived T lymphocytes are CD4 T$_{\alpha\beta}$ cells

To characterize the PBI-born T cell population, the GFP⁺ cells were sorted from the PBI- and AGM-labeled *Tg(hsp70 :mCherry-T2a-CreER^T2;lck:loxP-DsRedx-loxP-GFP)* larvae at 16 dpf (Fig. 2 A) and subjected to real-time quantitative PCR (qPCR) to examine the expression of T cell receptor α (*tcrα*) and δ (*tcrδ*; Haire et al., 2000; Schorpp et al., 2006). As expected, the expression of T cell receptors
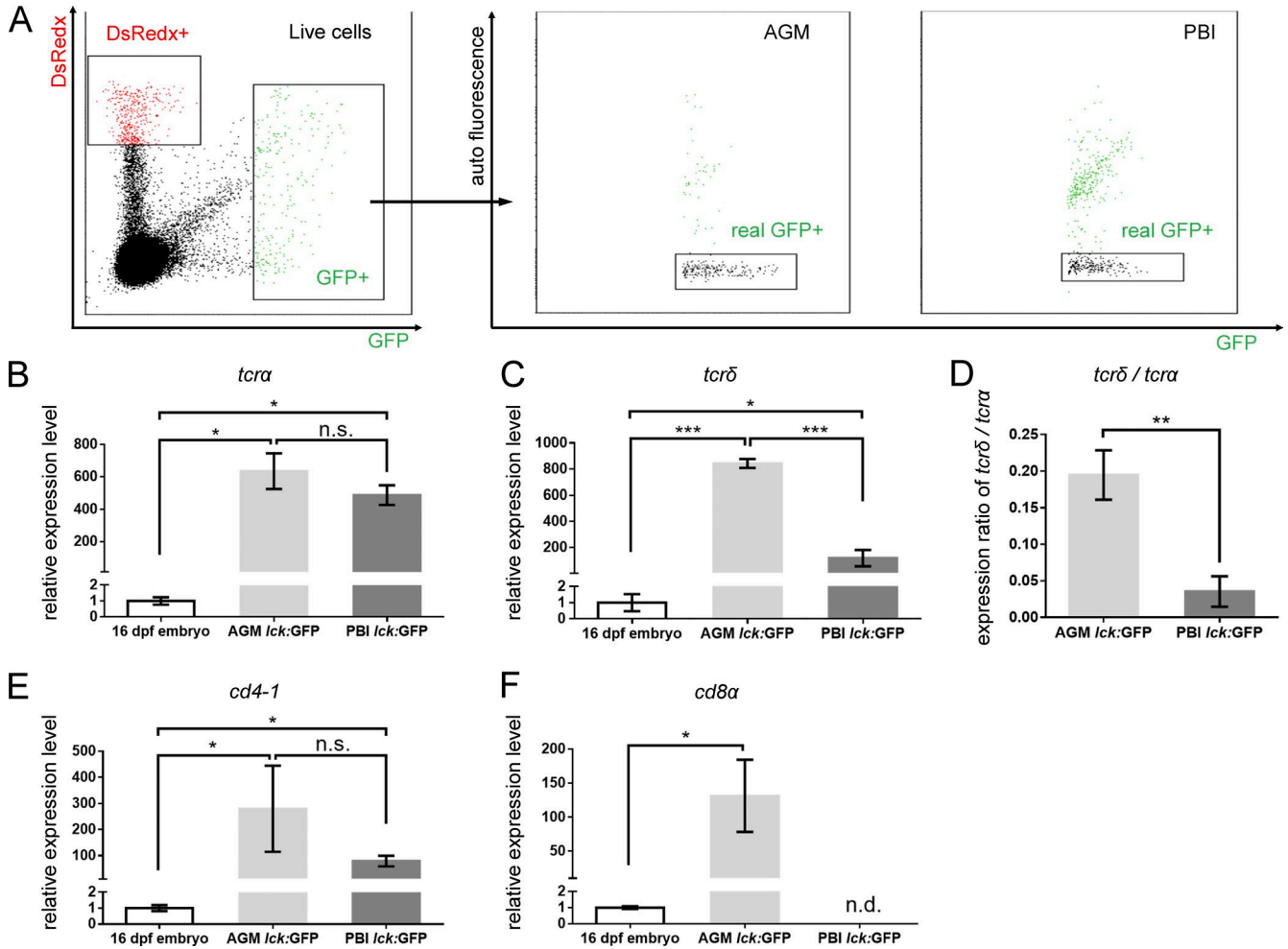
Figure 2. **Characterization of PBI-derived T cells.** (A) Dot plot of FACS of *lck*:GFP⁺ cells from 16-dpf AGM-irradiated (left) and PBI-irradiated (middle) fish. GFP⁺ cells are gated from live cells, and autofluorescent cells are excluded by real-GFP⁺ gate. Three independent experiments (in each group, ~20 fish are pooled together) are conducted. The cDNA are prepared from at least 250 *lck*:GFP⁺ cells isolated from 16-dpf AGM- and PBI-irradiated embryos and subjected to qPCR analysis. cDNA prepared from the whole 16-dpf embryos are used as a control. (B and C) Relative expression levels of *tcrα* and *tcrδ* in the AGM- and PBI-derived T cells. Three independent experiments are conducted. (D) Expression ratio of *tcrδ* to *tcrα*. The values are calculated on the basis of the expression level of *tcrα* and *tcrδ* relative to the internal control gene (*elf1a*). (E and F) Relative expression levels of *cd4-1* and *cd8α* in the AGM- and PBI-derived T cells. Three independent experiments are conducted. Data are represented as mean ± SD. Unpaired, two-tailed *t* test was performed to determine significance. *, $P < 0.05$; **, $P < 0.01$; ***, $P < 0.001$. See also Fig. S4.

(both α and δ) in both samples was much higher than that of 16-dpf whole embryo (Fig. 2, B and C), indicating that the sorted cells are highly enriched in T cells. Interestingly, we found that whereas the expression level of *tcrα* were comparable between the AGM- and PBI-derived T cells (Fig. 2 B), the *tcrδ* expression was about sevenfold higher in the AGM-derived T cells than that of the PBI-derived population (Fig. 2 C), suggesting that the AGM is the main resource of $T_{\gamma\delta}$ cells. In fact, the relative expression ratio of *tcrδ* versus *tcrα* in the PBI-derived T cells is only 3.5%, which is significantly lower than that (19.5%) in the AGM-derived T cells (Fig. 2 D). These data suggest that the PBI-derived T cells are predominantly $T_{\alpha\beta}$ cells.

To further characterize the PBI-derived $T_{\alpha\beta}$ cells, we next examined the expression of two other well-known T lympho-cyte subclass markers, CD4 and CD8 (Buchholz et al., 2016). Real-time qPCR analysis showed that both AGM-derived and PBI-derived T cells expressed high level of *cd4-1* (Fig. 2 E), the zebrafish counterpart of mammalian *CD4* (Yoon et al., 2015; Dee et al., 2016). In contrast, the *cd8α* (Somamoto et al., 2005; Takizawa et al., 2007) was robustly expressed in the AGM-derived T cells but not in the PBI-derived T cells (Fig. 2 F). Collectively, these results show that the zebrafish PBI generates a transient wave of CD4 $T_{\alpha\beta}$ cell population independent of HSCs. PBI-derived CD4 T cells appeared to be able to mature as they expressed other T cell markers such as *tcrβ2* and

3350

Distinct waves of T lymphopoiesis in zebrafish | Tian et al.

cd3ζ, which are crucial for T cell receptor signaling (Schorpp et al., 2006; Yoder et al., 2007; Fig. S4, B and C) and egressed from the thymus by 15 dpf (Fig. S4 A, arrows). In addition, Foxp3a, the master transcription factor essential for the development of regulatory T (T reg) cells (Mitra et al., 2010), was also detected in the PBI-derived CD4 T cells (Fig. S4 D), implying that they have the potential to differentiate into T reg cells.

PBI–derived T cells arise from caudal aorta endothelium

We next sought to determine which origin of the PBI-derived T cells arise from and when they emerge. It is well known that the PBI, which later forms the caudal hematopoietic tissue, a hematopoietic organ equivalent to mammalian fetal liver for fetal hematopoiesis (Murayama et al., 2006; Jin et al., 2007), are enriched in vasculature structures which consist of a caudal aorta (CA) and a caudal vein which later forms the caudal vein plexus (CVP; Isogai et al., 2001; Fig. 3 A). Previous studies have shown that the endothelium in the ventral wall of DA in the AGM directly produces HSCs through endothelial-hematopoietic transition (EHT; Bertrand et al., 2010; Kissa and Herbomel, 2010). We therefore hypothesized that the PBI-derived T cells are also originated from the endothelial cells in the ventral wall of CA. To test this hypothesis, we used the *Tg(flk1:dendra2)* transgenic line, in which the photoactivatable fluorescent protein Dendra2 (Gurskaya et al., 2006) is specifically expressed in the endothelial cells of vessels (Fig. 3 B). The endothelium in the dorsal and ventral wall of CA as well as the CVP (Fig. 3, D–F′) in the PBI were converted with a 405–nm UV laser at 26–28 hpf, before the AGM-derived hematopoietic cells colonize the PBI (Kissa and Herbomel, 2010). Right after the UV conversion, imaging was immediately performed to ensure the specificity of the photoconversion (Fig. 3, D–F′). The fate of the photoconverted endothelial cells (red fluorescence) was followed by direct observation under confocal fluorescent microscope (Fig. 3 B). In parallel, we also converted the endothelium of the ventral wall of DA in the AGM (Fig. 3, C and C′). As anticipated, as early as 3 dpf, abundant red–fluorescent progenies were found in the thymus of the embryos (7 of 8 embryos) photoconverted in the ventral endothelium of CA (Fig. 3 H), which was similar to the AGM DA-converted embryos (Fig. 3 G). In contrast, neither the CA dorsal endothelium–converted embryos (0 of 9 embryos) nor the CVP-converted embryos (0 out of 10 embryos) displayed any red–fluorescent progenies in the thymus (Fig. 3, I and J). These data indicate that the endothelium of the ventral wall of CA in the PBI is the source that generates the transient wave of T cells, presumably via the EHT. Indeed, time-lapse imaging showed that EHT occur in the ventral wall of CA from about 32 hpf until 72 hpf (Fig. 3, K–P; and Video 1). Collectively, these data demonstrate that the endothelium of the ventral wall of CA in the PBI is indeed capable of giving rise to a transient wave of T lymphopoiesis independent of HSCs via EHT. Because DA and CA are anatomically integrated as a single aorta channel, our data indicate that the ventral wall of aorta from the rostral end of DA to the caudal end of CA contains a consecutive hemogenic endothelial layer capable of giving rise to hematopoietic cells. We herein refer this hemogenic endothelial layer as hemogenic endothelium of aorta (HEA).

The AGM region generates HSC-independent T lymphocytes in situ

The consecutive layer of the HEA raises the possibility that the aorta endothelium in the AGM may also give rise to this transient wave of T cells independent of HSCs. To explore this possibility, we irradiated a small single spot (anterior, middle, and posterior, respectively) in the AGM of the *Tg(hsp70:mCherry–T2a–CreER^{T2};lck:loxP–DsRedx –loxP–GFP)* embryos at 22–24 hpf (Fig. 4 A), before the emergence of EHT to avoid mislabeling of hematopoietic precursors derived from HSCs. We assumed that in some of the infrared-irradiated embryos, only the endothelial cells capable of giving rise to HSC-independent T cells would be successfully labeled if the AGM endothelium indeed produced both HSCs and non-HSC hematopoietic precursors. If so, a transient appearance of GFP⁺ T cells in the thymus would be detected in these embryos. We therefore collected all the embryos with GFP⁺ signals in the thymus at 5 dpf and monitored the dynamic behaviors of these GFP⁺ T cells at 40 dpf and adulthood. Consistent with our prediction, whereas a large portion of the infrared-irradiated fish (category I) contained GFP⁺ T cells in the larvae (5 dpf), juveniles (40 dpf) and adult fish (Fig. 4, B–D; and Fig. S5, A and B; indicating successful labeling of HSCs in these fish), a substantial number of the irradiated fish (category II) displayed a transient wave of T lymphopoiesis: the GFP⁺ T cells were abundant in the larvae but absent in the juveniles and adult fish (Fig. 4, E–G; and Fig. S5, A and B). This dynamic pattern in category II fish is identical to that of the transient wave of T lymphopoiesis observed in the PBI-irradiated fish (Fig. 1 C). These findings indicate that in addition to giving rise to HSCs, the AGM also produces hematopoietic precursors capable of generating a transient wave of T lymphopoiesis. Interestingly, the percentage of category I fish gradually reduced from the anterior (73 ± 3.6%) to the posterior (30 ± 10.2%) of the AGM and eventually became hardly noticed in the PBI (2.4 ± 4.1%; Fig. 4 H), which is consistent with previous data showing that the PBI does not in situ generates HSCs (Fig. 1 and Figs. S1 and S2). This result indicates that the frequency of HSC production along the HEA is uneven and displays a gradient pattern from the anterior to the posterior.

### The HSC–independent and HSC–dependent T lymphocytes emerge in successive waves

The existence of HSC-independent T lymphopoiesis prompted us to investigate whether the HSC-derived and HSC-independent T lymphopoiesis emerge simultaneously or at distinct time windows. To answer this question, we used the *Tg(hsp70:mCherry–T2a–CreER^{T2};lck:loxP–DsRedx–loxP–*
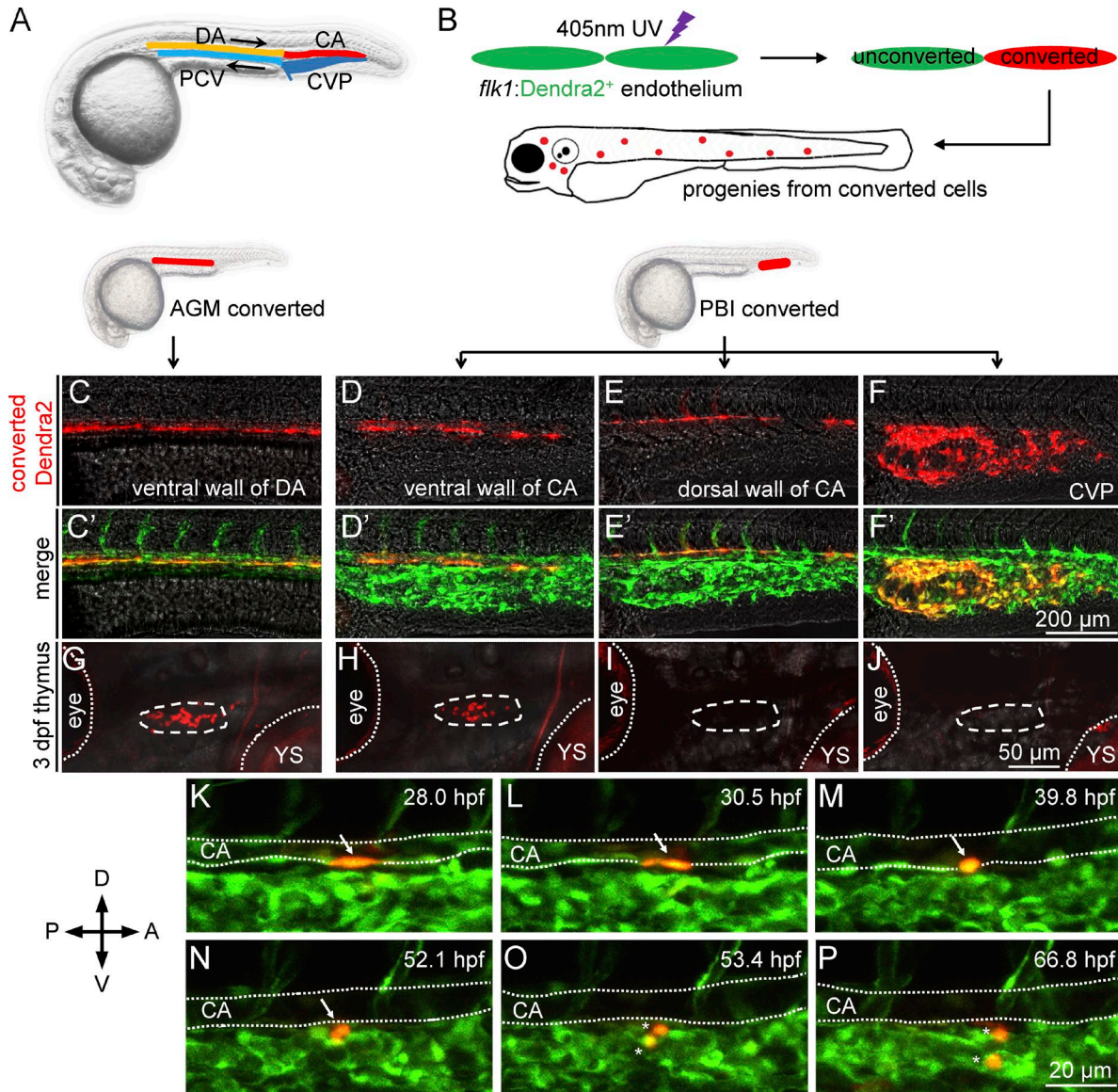
Figure 3. PBI–derived T cells originate from the ventral endothelium of caudal aorta. (A) A schematic diagram of the anatomy of main blood vessels in 28-hpf zebrafish embryos. CA, caudal aorta (red); CVP, caudal vein plexus (dark blue); DA, dorsal aorta (orange); PCV, posterior cardinal vein (light blue). Black arrows indicate direction of blood flow. (B) A schematic diagram of photoconversion of *flk1*:Dendra2+ vessel endothelial cells in 28 hpf *Tg(flk1 :Dendra2+)* embryos. Fluorescent color of Dendra2 changes from green to red after exposure to 405-nm UV laser. (C–F) Red fluorescence of Dendra2+ cells after photoconversion at 28 hpf. The ventral wall of DA, the ventral wall of CA, the dorsal wall of CA, and the CVP are photoconverted using 405-nm UV laser. Fluorescence images are captured immediately after photoconversion. (C'–F') Merged images of converted (red) and unconverted (green) endothelial cells corresponding to C–F. (G–J) Red Dendra2 signals in the thymus of photoconverted fish. Red Dendra2 signals are detected in the thymus of the 3-dpf embryos photoconverted in the ventral wall of DA (4 of 4) and ventral wall of CA (7 of 8) but not those photo-converted in the dorsal wall of CA (0 of 9) or the CVP (0 of 10). Dashed circles depict the thymus. Dotted lines depict the boundaries of the eyes and YS. (K–P) Time-lapse confocal imaging of the PBI region of *Tg(flk1:Dendra2)* embryo after photoconversion. A photoconverted endothelial cell (arrows) in the ventral wall of CA undergoes EHT and subsequently divides into two daughter cells (asterisks). The endothelial cell is converted at 28 hpf and traced for ~40 h. The lumens of CA are depicted by dotted lines. A, anterior; D, dorsal; P, posterior; V, ventral.

GFP) reporter line and irradiated one single spot in the anterior of the AGM and one single spot in the PBI at 22–24 hpf, respectively (Fig. 5 A). We expected that we would be able to recover fish in which only the endothelium that gives rise to HSCs or HSC-independent T progenitor cells were labeled. At 5 dpf, the irradiated embryos were separated into two groups according to the presence (5-dpf–GFP+ group) or absence (5-dpf–GFP− group) of GFP+ cells in the thymus. The
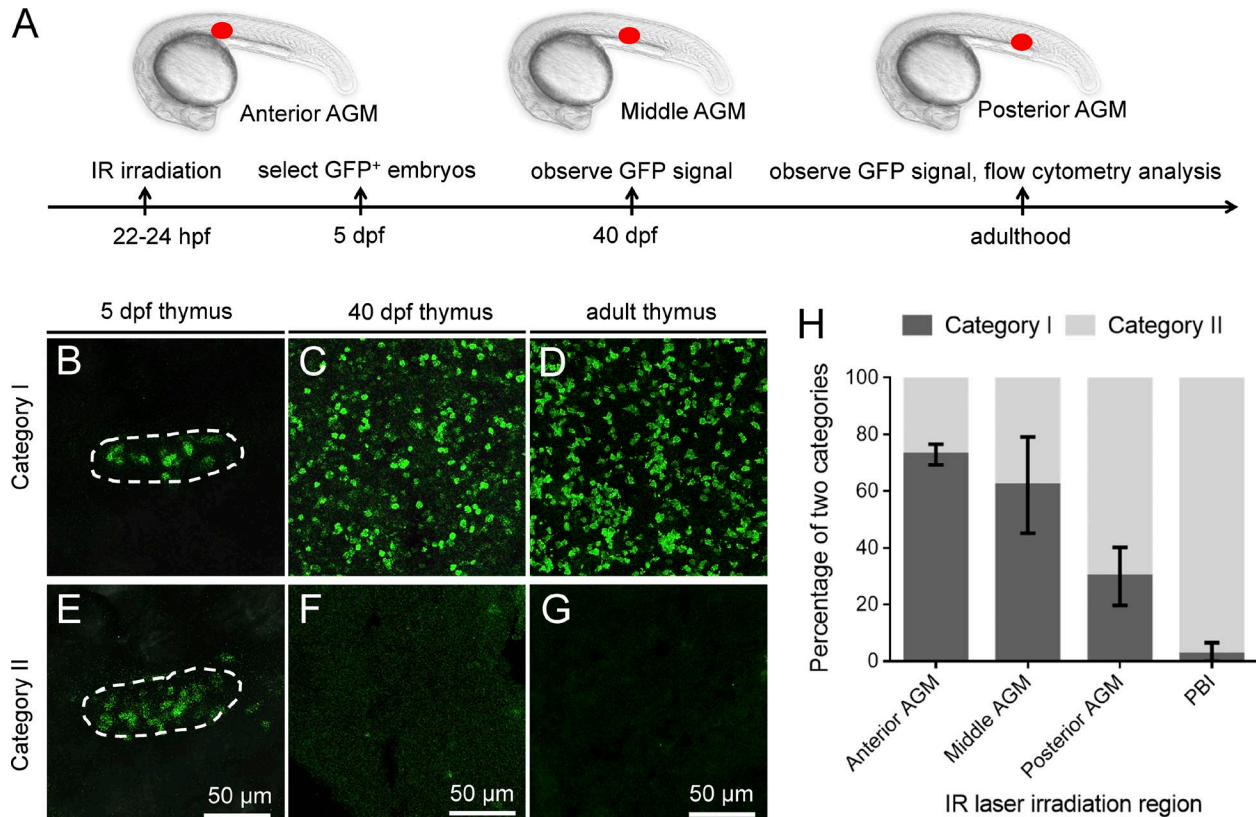
Figure 4. **The AGM in situ generates HSC–independent T cells.** (A) A schematic diagram of the experimental design. 22- to 24-hpf double-transgenic *Tg(hsp70:mCherry-T2a-CreER^{T2};lck:loxP-DsRedx-loxP-GFP)* embryos are irradiated in the anterior (somite 7), middle (somite 11), and posterior (somite 15; red dot) of the AGM region and subsequently treated with 4-hydroxytamoxifen. At 5 dpf, embryos containing *lck*:GFP^+ cells in the thymus are selected and survived to 40 dpf and adulthood for further analysis. IR, infrared. (B–D) Images of *lck*:GFP^+ cells in the thymus of category I fish, in which GFP^+ T cells are maintained from embryonic stage to adulthood. Dashed line depicts the thymus of 5-dpf embryos. (E–G) Images of *lck*:GFP^+ cells in the thymus of category II fish, in which GFP^+ T cells are present at 5 dpf but absent at 40 dpf and adulthood. Dashed line depicts the thymus of 5 dpf embryos. (H) Percentage of category I and category II fish in total fish irradiated in the PBI and in the anterior, middle, and posterior of the AGM. Three independent experiments are conducted [(experiment 1: anterior AGM, $n = 4$; middle AGM, $n = 8$; posterior AGM, $n = 13$; and PBI, $n = 14$); (experiment 2: anterior AGM, $n = 16$; middle AGM, $n = 19$; posterior AGM, $n = 20$; and PBI, $n = 16$); (experiment 3: anterior AGM, $n = 12$; middle AGM, $n = 7$; posterior AGM, $n = 12$; and PBI, $n = 14$)]. Data are represented as mean $\pm$ SD. See also Fig. S5.

embryos were then grown to the desired stages and subjected to further examination (Fig. 5 A). Consistent with previous data (Fig. 4 H and Fig. S1 B), in the 5-dpf-GFP^+ group of anterior AGM-irradiated fish, 68% maintained GFP^+ cells from 5 dpf to adulthood (Fig. 5 C, orange line), whereas all the 5-dpf-GFP^+ PBI-irradiated fish (as well as 32% of anterior AGM-irradiated fish) lost the GFP signals by 40 dpf (Fig. 5 C, dark blue line and orange line). Strikingly, in the 5-dpf-GFP^− group of anterior-AGM irradiated fish, 64% began to acquire GFP^+ cells in the thymus from 8 dpf onward and continued to maintain GFP^+ T cells to adulthood (Fig. 5, B and C, red line). In contrast, fish in 5-dpf-GFP^− group of PBI irradiation did not acquire GFP^+ T cells at later stage (Fig. 5, B and C, light blue line). These results indicate that the late-emerged GFP^+ T cells are derived from HSCs but not HSC-independent lymphopoiesis. These results also suggest that the T cells colonized the thymus before 8 dpf are not derived from HSCs

but rather solely from the transient wave of T lymphopoiesis. The comparable percentage of the HSC-labeled fish in 5-dpf-GFP^+ (68%) and 5-dpf-GFP^− group (64%) of AGM-irradiated fish (Fig. 5 C) indicated that presence of GFP^+ cells at 5 dpf and labeling of HSCs are statistically independent, which further supports that HSCs do not contribute to the lymphopoiesis before 8 dpf. Taken together, these data indicate that in the HSC-independent T cells emerge early at 3 dpf (Fig. 3 H) and last transiently until juvenile stage, whereas HSC-derived T cells emerge later at around 8 dpf and continuously maintain to adulthood. In accord with this conclusion, the AGM-derived T cells isolated before 6 dpf were predominantly CD4 T_{αβ} cells, which are identical to the PBI-derived T cells (Fig. 5 D). Collectively, our study demonstrates that HSC-independent T cells and HSC-derived T cells emerge at distinct time windows, indicating the importance of HSC-independent T cells in early embryonic stage when HSC-derived T cells are absent.
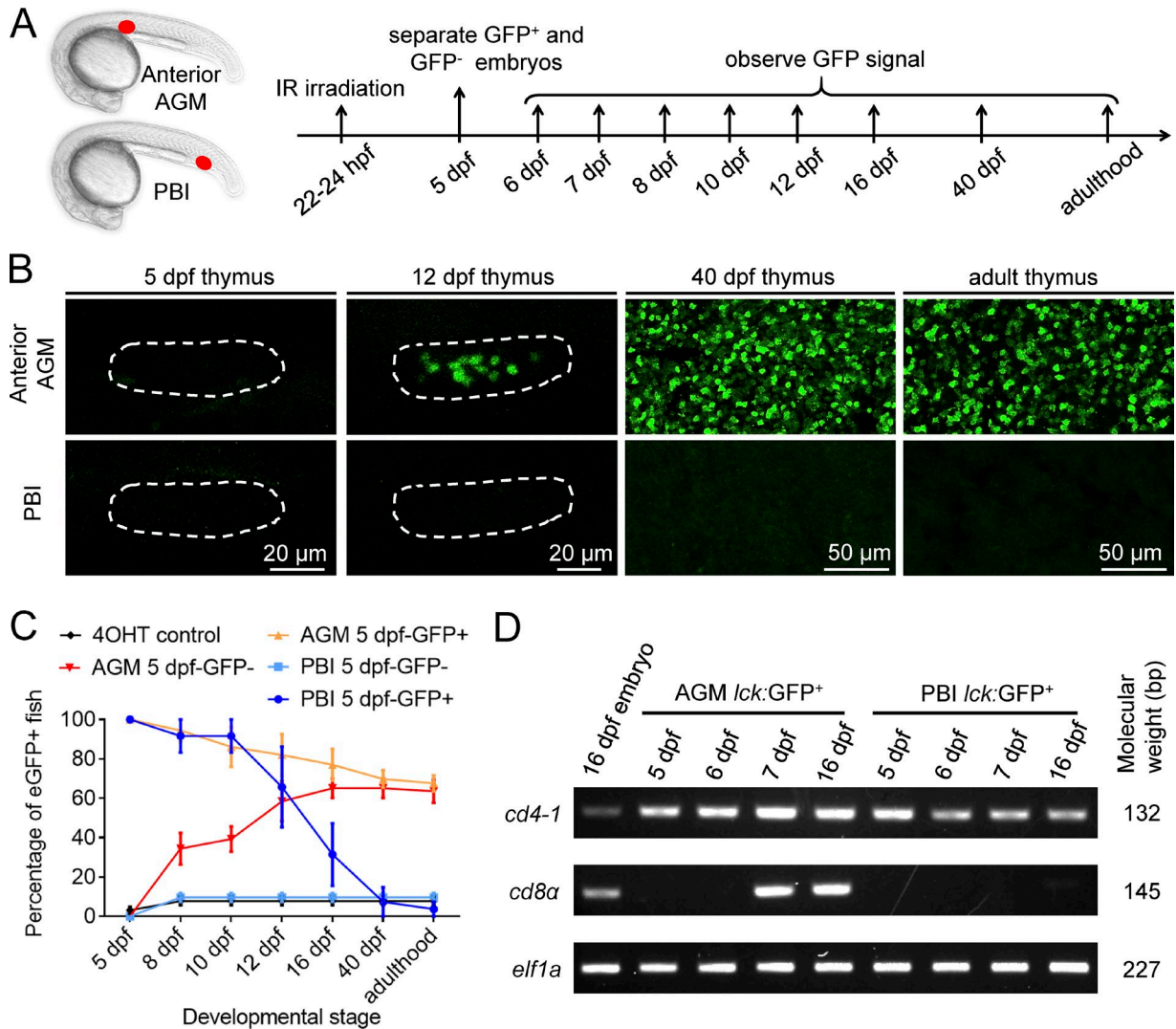
Figure 5. **HSC–derived and HSC–independent T cells develop in successive waves.** (A) A schematic diagram of the experimental design. 22- to 24-hpf double-transgenic *Tg(hsp70:mCherry-T2a-CreER^T2;lck:loxP-DsRedx-loxP-GFP)* embryos are irradiated in the anterior of the AGM (red dot) and the PBI (red dot) flowed by 4-hydroxytamoxifen (4-OHT) treatment. At 5 dpf, the irradiated embryos are separated according to the presence (5-dpf-GFP+) or absence (5-dpf-GFP−) of *lck*:GFP+ cells in the thymus. The presence of *lck*:GFP+ cells in the thymus and their dynamic behavior are monitored at the indicated stages. (B) Images of *lck*:GFP+ cells in the thymus of 5-dpf-GFP− group fish at various stages. Most of the AGM-irradiated 5-dpf-GFP− fish begin to acquire GFP+ T cells from 8 dpf onward and continue to maintain GFP+ T cells to adulthood. The PBI-irradiated 5-dpf-GFP− fish do not contain GFP+ T cells at all the time window examined. Dashed line depicts the thymus of 5- and 12-dpf embryos. (C) Percentage of GFP+ fish of each group at various stages. Control group (black line), AGM-irradiated 5-dpf-GFP− group (red line), AGM-irradiated 5-dpf-GFP+ group (orange line), PBI-irradiated 5-dpf-GFP− group (light blue line), and PBI-irradiated 5-dpf-GFP+ group (dark blue line) are shown. Three independent experiments are conducted (experiment 1: anterior AGM, $n = 20$; PBI, $n = 25$; and 4-OHT control, $n = 22$; experiment 2: anterior AGM, $n = 25$; PBI, $n = 17$; and 4-OHT control, $n = 17$; experiment 3: anterior AGM, $n = 61$; PBI, $n = 13$; and 4-OHT control, $n = 28$). Data are represented as mean ± SD. (D) Expression of *cd4-1* and *cd8α* in the PBI- and AGM-derived *lck*:GFP+ T cells at various stages detected by RT-PCR. *elf1a* is used as internal control.

DISCUSSION

In this study, we have unambiguously demonstrated that zebrafish aorta endothelium gives rise to two successive waves of T lymphopoiesis: an early transient wave producing predominantly CD4 $T_{\alpha\beta}$ cells during embryonic and larval stages in an HSC-independent manner, and a late definitive wave generating all T cell subclasses from larval stage to adulthood via the differentiation of HSCs (Fig. 6).

Using a temporal–spatial resolved cell fate mapping, our study has provided explicit in vivo evidence demonstrating that the zebrafish aorta endothelium in the AGM and PBI regions generates a transient wave of T cells independent of HSCs.
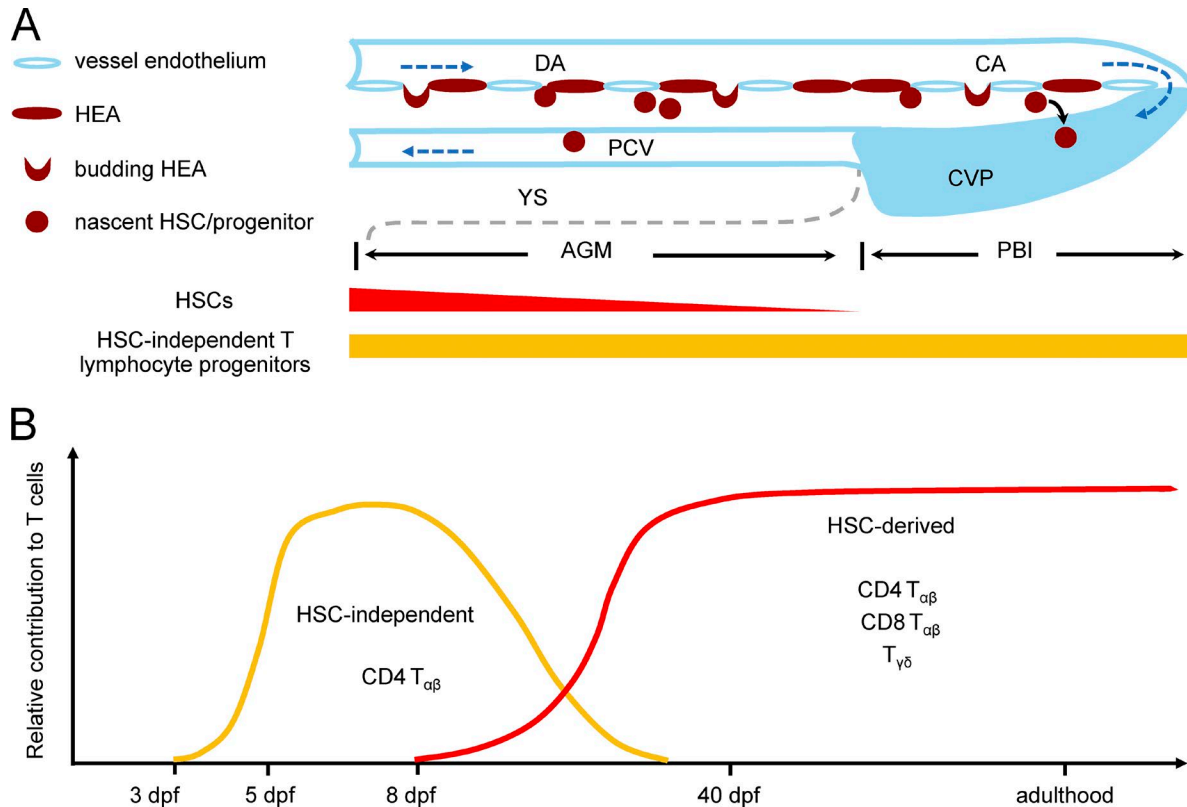
Figure 6. **Summary of distinct waves of T lymphopoiesis in zebrafish.** (A) A schematic diagram illustrates that EHT occurs along the entire ventral endothelium of the aorta in zebrafish. Blood vessels are marked by light blue. Direction of blood flow is indicated by dark blue dashed arrows. Boundary of the yolk sac in the ventral side of the trunk is depicted by gray dashed line. Hemogenic endothelium of aorta (HEA) is indicated in dark red. The capacity of generating HSCs and HSC-independent T cell progenitors along the HEA are indicated by red and orange bar, respectively. (B) A schematic diagram depicts two waves of T lymphopoiesis in zebrafish. HSC-independent T cells (orange) emerge at 3 dpf and gradually decline at the late larval stages and diminish in juvenile and adulthood. HSC-derived T cells (red) emerge at around 8 dpf and are replenished continuously throughout the life span of zebrafish.

Our results are in agreement with previous studies in mouse models, which have suggested that T lymphoid progenitors can be detected before the emergence of HSCs (Yoshimoto et al., 2012; Böiers et al., 2013). Yet unlike zebrafish, these early-emerged T lymphoid cells in mice are thought to arise from the YS rather than the AGM because precursors with T lymphoid potential appear to be detected in the YS as early as E9.5, and the VE-cad$^+$CD41$^-$ endothelial cells in the E9-9.5 YS can give rise to T lymphoid lineage, when co-cultured with OP9–DL1 cells in vitro. The discrepancy of the origin of the early-emerged T cells between zebrafish and mammals could be due to the species difference, so that the production of HSCs and HSC-independent hematopoietic precursors is separated into different tissues during evolution. Alternatively, like zebrafish, the mammalian AGM endothelium is also capable of giving rise to a transient wave of T lymphopoiesis independent of HSCs. In fact, because the conclusions from those mouse studies are based on either in vitro assays or transplantation assays lacking precise lineage tracing, the possibility that HSC-independent hematopoietic progenitors arise directly from the AGM endothelium cannot be excluded. It will be

of great interest to reinvestigate this issue in mammals using a temporal–spatial restricted fate-mapping analysis.

Recently, Beaudin et al. (2016) identified that Flk2$^+$ hematopoietic precursors, which are present in the mouse YS, AGM, and fetal liver but absent in adulthood, can give rise to innate-like lymphocytes. Although the Flk2$^+$ hematopoietic precursors exhibit long-term multilineage potential when transplanted into the recipient mice, a cell fate mapping study indicated that the Flk2$^+$ hematopoietic precursors appear to emerge independent of conventional HSCs (Boyer et al., 2011). Considering the transient appearance in multiple hematopoietic tissues (YS, AGM, and fetal liver) and lymphoid-priming of the Flk2$^+$ cells, we speculate that this Flk2$^+$ hematopoietic population could be the counterpart of the zebrafish non-HSC-derived hematopoietic precursors capable of giving rise to the early transient wave of T lymphopoiesis, because our study has revealed that the non-HSC-derived hematopoietic precursors in zebrafish also arise from multiple regions (the AGM and PBI) of the aorta. The discrepancies of these two populations such as their lineage and long-term renewal potentials could be attributed to

the differences in the experimental assays used in these different studies. It will be of great interest to perform an in vivo fate-mapping analysis of Flk2^{+} cells in mice and, conversely, a cell transplantation assay with these non–HSC-derived hematopoietic precursors in zebrafish.

Our study documents that the ventral endothelium of the entire aorta, from the anterior of the AGM to the posterior of the PBI, can give rise to hematopoietic cells via EHT. This is in agreement with previous studies in mouse models showing that the endothelium in the YS, AGM, placenta, and embryonic head region are all capable of producing HSCs and hematopoietic progenitors (Alvarez-Silva et al., 2003; Gekas et al., 2005; Ottersbach and Dzierzak, 2005; Li et al., 2012). It will be of great interest to investigate the hematopoietic potential of the vessel endothelium in different tissues in mammals using a temporal–spatial resolved fate-mapping strategy. Notably, our study also shows that the hemogenic endothelium in the anterior and posterior of the zebrafish aorta manifests distinct hematopoietic potential (the ability of giving rise to HSCs reduces from the anterior to posterior of aorta, whereas the ability of generating HSC-independent T cells appears to be broadly maintained). Although the underlying molecular basis remains unknown, two possible mechanisms could achieve such dynamic potential. One explanation is that this is determined by an intrinsic genetic program, in which the anterior and posterior of the aorta consist of different numbers of hemogenic endothelium capable of giving rise to HSCs and HSC-independent T cells. Alternatively, the distinct hematopoietic potential of the hemogenic endothelium of the aorta is dictated by extrinsic signals specifically produced by the different niches. Currently, several signaling pathways are implicated to play critical roles in the fate determination and emergences of HSCs. The Notch and proinflammatory pathways are the two most notable signaling cascades involved in HSC development (Burns et al., 2005; Espín-Palazón et al., 2014; He et al., 2015; Butko et al., 2016; Kanz et al., 2016). Likewise, biomechanical force and the NO pathway, which can be promoted by blood flow, are also shown to participate in the formation of HSCs (Adamo et al., 2009; North et al., 2009). Recently, Monteiro et al. (2016) found that the TGFβ signaling cascade is required for the emergence of HSCs, possibly via modulating the Notch pathway. We speculate that the interplays of these different signaling pathways not only determine the emergence of HSCs but also dictate the formation of the non–HSC precursors from the aorta endothelium. Further mechanistic studies will be necessary to clarify this issue.

Previous studies have shown that the CA and CVP, together with perivascular mesenchymal stromal cells in the PBI, form a hematopoietic niche that transiently accommodates HSCs migrated from the AGM and modulates their subsequent proliferation and differentiation (Murayama et al., 2006; Jin et al., 2007, 2009; Tamplin et al., 2015). Our study has documented that the ventral endothelium of CA generates hematopoietic precursors capable of giving rise to T

cells, demonstrating that this region not only functions as a transitory tissue for the accommodation, expansion, and differentiation of HSCs but also as a source for generating a transient wave of T lymphopoiesis. Notably, a previous study by Bertrand et al. (2007) revealed that the PBI can also give rise to EMPs. Further in vitro culture, cell transplantation, and lineage-tracing analysis have confirmed that, similar to mammalian EMPs (Frame et al., 2013; Lin et al., 2014), zebrafish EMPs are capable of differentiating into erythroid and myeloid cells but not T cell lineage (Bertrand et al., 2007). On the basis of these results, we speculate that the HSC-independent T cells and EMPs are likely derived from aorta endothelium independently, although a common precursor cannot be excluded. Finally, given that the AGM can generate both HSCs and non–HSC precursors capable of giving rise to T cells independently, we suspect that the zebrafish AGM endothelium may also produce EMPs via EHT.

The identification of the transient wave of HSC-independent T cells raises an important question: what are the biological functions of the early-emerged T cell population? Previous studies in human samples have suggested that fetal T cells appear to display much higher responsiveness to allogenic stimulations and the CD4^{+} population in fetal T cells are more likely to adopt T reg cell fate (Mold et al., 2010), suggesting that fetal T cells may play a role in promoting immune tolerance in human fetuses (Michaëlsson et al., 2006; Mold et al., 2008, 2010). Given the high degree of similarity of the blood system between zebrafish and mammals, it is conceivable to speculate that the HSC-independent T cells we have identified in zebrafish may play an immune-repressive function. Consistence with this hypothesis, our results show that the HSC-independent T cells are largely CD4 helper T cells and are positive for *foxp3a*, a master regulator of T reg cells, suggesting that the HSC-independent T cells have the potential to differentiate into CD4 T reg cells under proper condition. Finally, it is well known that the interactions between thymocytes and thymic epithelial cells are critical for the development and maturation of the thymus organ (Klug et al., 2002; Langenau and Zon, 2005; Hess and Boehm, 2012). We therefore speculate that these early-emerged HSC-independent T cells may play a critical role during thymus organogenesis.

MATERIALS AND METHODS
Zebrafish
All zebrafish lines were maintained following standard protocol (Westerfield, 2000). In this study, AB WT, *Tg(lck:loxP-DsRedx-loxP-GFP)*, *Tg(flk1:Dendra2)*, *Tg(coro1a:loxP-DsRedx-loxP-GFP)*hkztg12 (Xu et al., 2015), *Tg(hsp70:mCherry-T2a-CreERT2)#12* (Hans et al., 2011; a gift from M. Brand, Technische Universitaet Dresden, Dresden, Germany), *Tg(ubi:loxP-GFP-loxP-mCherry)* (Mosimann et al., 2011; a gift from L.I. Zon, Howard Hughes Medical Institute, Harvard Medical School, Children's Hospital, Boston, MA) and *runx1[W84X]* (Jin et al., 2009; Sood et al.,

2010) were used. All animal procedures and experiments were conducted according to the guidelines of the Animal and Plant Care Facility of the Hong Kong University of Science and Technology (HKUST). All the animal experiments were approved by the Animal Ethics Committee of HKUST.

Infrared–mediated temporal–spatial resolved cell labeling

The infrared–mediated temporal–spatial resolved cell labeling system was described previously (Xu et al., 2015). Heat-shock–mediated cell labeling by infrared laser was manipulated according to the previous study (Xu et al., 2015).

Generation of transgenic lines

The promoter of *lck* gene was cloned according to a previous study (Langenau et al., 2004) and replaces the *coro1a* promoter on coro1a:loxP-DsRedx-loxP-GFP construct (Xu et al., 2015). The promoter of α/β_{a2}-*globin* was cloned according to a previous study (Ganis et al., 2012) and replaces the *coro1a* promoter on coro1a:loxP-DsRedx-loxP-GFP construct (Xu et al., 2015). The resulting lck:loxP-DsRedx-loxP-GFP construct and globin:loxP-DsRedx-loxP-GFP construct were respectively injected into single-cell stage AB WT zygotes together with mRNA of transposase (Kawakami et al., 2000).

Cryosection, immunofluorescent antibody staining, and imaging

Fish were anesthetized on ice and fixed in 4% PFA at room temperature for 1 d. After washing with PBS at room temperature for 1–2 d, samples were soaked in coagulating solution (1.5% agar + 5% sucrose) and were dehydrated in 30% sucrose for 3 d. The cryosection of dehydrated samples was performed at 16-μm thickness. Immunohistochemistry on section samples was performed as previously described (Wendl et al., 2002). Primary antibodies used in this study are anti–GFP antibody (ab6658; Abcam), anti–DsRedx antibody (632496; Clontech), and anti–α_{e1}-Globin (Jin et al., 2007). Secondary antibodies used in this study are Alexa Fluor 555–anti–rabbit antibody (A31572; Invitrogen) and Alexa Fluor 488–anti–goat antibody (A11055; Invitrogen). Imaging of fluorescent signals in young larvae and in skin was conducted on anesthetized fish using a Leica SP8 confocal microscope.

Whole–mount in situ hybridization

Antisense DIG-labeled *lyz* RNA probe was synthesized in vitro. Fish were anesthetized on ice and fixed in 4% PFA at room temperature for 2 h. The staining process followed a previous study (Thisse and Thisse, 2008) to detect the signals.

Photoconversion fate mapping and time–lapse imaging

Endothelial cells in *Tg(flk1:Dendra2)* were converted by 405–nm UV laser at 28 hpf, as previously described (Dixon et al., 2012). The photoconverted endothelial cells were imaged immediately after photoconversion, and the Dendra2^{+} progenies in the thymus were captured at 3 dpf. Time-lapse imaging of EHT in the PBI of *Tg(flk1:Dendra2)* embryos was performed from 28–96 hpf according to a previous study (Xu et al., 2016). Time-lapse imaging of fluorescent signals was captured using a Leica SP8 confocal microscope.

Flow cytometry analysis

The kidney marrow and spleen of adult fish were dissected and homogenized by grinding on the 40-μm nylon mesh in 5% FBS/PBS solution. The cell suspensions were then subjected to flow cytometry analysis according to a previous study (Stachura and Traver, 2016). *Tg(hsp70:mCherry-T2a-CreERT2;lck:loxP-DsRedx-loxP-GFP)*, *Tg(hsp70:mCherry-T2a-CreERT2;globin:loxP-DsRedx-loxP-GFP)*, and *Tg(hsp70:mCherry-T2a-CreERT2;ubi:loxP-GFP-loxP-mCherry)* fish were analyzed by flow cytometry (FACS Aria IIIu; BD Bioscience).

FACS, cDNA synthesis, and qPCR

The embryos irradiated in the AGM and PBI were collected at 5, 6, 7, and 16 dpf, and at least 20 embryos irradiated in the same region were pooled together and homogenized by needles and syringes. The homogenized samples were then treated with 0.25% Trypsin-EDTA (25200-072; Gibco) at 30°C for 30 min and stopped by adding calcium chloride. Suspended cells were collected by centrifugation (400 *g* at 4°C), filtered by 35-μm nylon mesh (352235; FALCON), and finally subjected to FACS (FACS Aria IIIu). The cDNA was prepared from sorted GFP^{+} cells and amplified by Smart-seq2 according to previous studies (Picelli et al., 2013, 2014). Real-time qPCR was performed to examine the transcripts corresponding to the coding region of *cd4-1*, *cd8α*, *foxp3a*, and *cd3ζ* and the constant region of *tcrα*, *tcrβ2*, and *tcrδ*. Primers for qPCR are listed as follows: *tcrα* FP 5′-ACGTCGGCTGTCCGATATTCA-3′; *tcrα* RP 5′-GCCCAGTGACAAGAAGTTGAC-3′; *tcrβ2* FP 5′-CCAACAATAAATTCACCTGCAC-3′; *tcrβ2* RP 5′-CAGACACAACCAGTGCATAC-3′; *tcrδ* FP 5′-CGGCTACACTTGAATGTCAC-3′; *tcrδ* RP 5′-CTGCAACACATTTAGCCAGC-3′; *cd4-1* FP 5′-GGTGTTTGGACATGCCAGTTG-3′; *cd4-1* RP 5′-GCTGACTGTCGAGGATTGAG-3′; *cd8α* FP 5′-GCAAAAAGGACAGACAGCGG-3′; *cd8α* RP 5′-CAACAGGCTTCAGTGTTGTTTG-3′; *foxp3a* FP 5′-ACTGTGCCACCTTTTCCATCA-3′; *foxp3a* RP 5′-TCTGAGGTCACTCTCCAAGG-3′; *cd3ζ* FP 5′-CGTGCAGATGAGACGTACAC-3′; *cd3ζ* RP 5′-GTACGTGTCTTTGGTGACCG-3′; *elf1a* FP 5′-TACTTCTCAGGCTGACTGTG-3′; and *elf1a* RP 5′-ATCTTCTTGATGTATGCGCT-3′.

Statistical analysis

The *F* test was performed to test two-sample variances. According to the results of the *F* test, the two-sample *t* test was performed assuming equal or unequal variances. Statistical analysis was performed using the Data Analysis tool in Excel (Microsoft). Two-tailed p-values were used in all *t* tests.

Online supplemental material

Fig. S1 shows that PBI–derived T cells are absent at juvenile and adulthood in multiple organs. Fig. S2 shows that PBI is not capable of generating HSCs in situ. Fig. S3 shows that PBI can in situ generate myeloid and erythroid cells but not B lymphocytes. Fig. S4 shows that both AGM- and PBI–derived T lymphocytes can develop into mature T cells. Fig. S5 shows that AGM single spot-irradiated fish display two distinct patterns of *lck*:GFP^{+} T cells in multiple organs. Video 1 shows the EHT in the PBI of *Tg(flk1:Dendra2)* embryos.

REFERENCES

Adamo, L., O. Naveiras, P.L. Wenzel, S. McKinney-Freeman, P.J. Mack, J. Gracia-Sancho, A. Suchy-Dicey, M. Yoshimoto, M.W. Lensch, M.C. Yoder, et al. 2009. Biomechanical forces promote embryonic haematopoiesis. *Nature.* 459:1131–1135. http://dx.doi.org/10.1038/nature08073

Alvarez-Silva, M., P. Belo-Diabangouaya, J. Salaün, and F. Dieterlen-Lièvre. 2003. Mouse placenta is a major hematopoietic organ. *Development.* 130:5437–5444. http://dx.doi.org/10.1242/dev.00755

Beaudin, A.E., S.W. Boyer, J. Perez-Cunningham, G.E. Hernandez, S.C. Derderian, C. Jujjavarapu, E. Aaserude, T. MacKenzie, and E.C. Forsberg. 2016. A transient developmental hematopoietic stem cell gives rise to innate-like B and T cells. *Cell Stem Cell.* 19:768–783. http://dx.doi.org/10.1016/j.stem.2016.08.013

Bertrand, J.Y., A.D. Kim, E.P. Violette, D.L. Stachura, J.L. Cisson, and D. Traver. 2007. Definitive hematopoiesis initiates through a committed erythromyeloid progenitor in the zebrafish embryo. *Development.* 134:4147–4156. http://dx.doi.org/10.1242/dev.012385

Bertrand, J.Y., N.C. Chi, B. Santoso, S. Teng, D.Y. Stainier, and D. Traver. 2010. Haematopoietic stem cells derive directly from aortic endothelium during development. *Nature.* 464:108–111. http://dx.doi.org/10.1038/nature08738

Böiers, C., J. Carrelha, M. Lutteropp, S. Luc, J.C. Green, E. Azzoni, P.S. Woll, A.J. Mead, A. Hultquist, G. Swiers, et al. 2013. Lymphomyeloid contribution of an immune-restricted progenitor emerging prior to definitive hematopoietic stem cells. *Cell Stem Cell.* 13:535–548. http://dx.doi.org/10.1016/j.stem.2013.08.012

Boyer, S.W., A.V. Schroeder, S. Smith-Berdan, and E.C. Forsberg. 2011. All hematopoietic cells develop from hematopoietic stem cells through Flk2/Flt3-positive progenitor cells. *Cell Stem Cell.* 9:64–73. http://dx.doi.org/10.1016/j.stem.2011.04.021

Buchholz, V.R., T.N. Schumacher, and D.H. Busch. 2016. T cell fate at the single-cell level. *Annu. Rev. Immunol.* 34:65–92. http://dx.doi.org/10.1146/annurev-immunol-032414-112014

Burns, C.E., D. Traver, E. Mayhall, J.L. Shepard, and L.I. Zon. 2005. Hematopoietic stem cell fate is established by the Notch-Runx pathway. *Genes Dev.* 19:2331–2342. http://dx.doi.org/10.1101/gad.1337005

Butko, E., C. Pouget, and D. Traver. 2016. Complex regulation of HSC emergence by the Notch signaling pathway. *Dev. Biol.* 409:129–138. http://dx.doi.org/10.1016/j.ydbio.2015.11.008

Cumano, A., F. Dieterlen-Lievre, and I. Godin. 1996. Lymphoid potential, probed before circulation in mouse, is restricted to caudal intraembryonic splanchnopleura. *Cell.* 86:907–916. http://dx.doi.org/10.1016/S0092-8674(00)80166-X

Cumano, A., J.C. Ferraz, M. Klaine, J.P. Di Santo, and I. Godin. 2001. Intraembryonic, but not yolk sac hematopoietic precursors, isolated before circulation, provide long-term multilineage reconstitution. *Immunity.* 15:477–485. http://dx.doi.org/10.1016/S1074-7613(01)00190-X

Dee, C.T., R.T. Nagaraju, E.I. Athanasiadis, C. Gray, L. Fernandez Del Ama, S.A. Johnston, C.J. Secombes, A. Cvejic, and A.F. Hurlstone. 2016. CD4-transgenic zebrafish reveal tissue-resident Th2- and regulatory T cell-like populations and diverse mononuclear phagocytes. *J. Immunol.* 197:3520–3530. http://dx.doi.org/10.4049/jimmunol.1600959

Dixon, G., P.M. Elks, C.A. Loynes, M.K. Whyte, and S.A. Renshaw. 2012. A method for the in vivo measurement of zebrafish tissue neutrophil lifespan. *ISRN Hematol.* 2012:915868. http://dx.doi.org/10.5402/2012/915868

Espín-Palazón, R., D.L. Stachura, C.A. Campbell, D. García-Moreno, N. Del Cid, A.D. Kim, S. Candel, J. Meseguer, V. Mulero, and D. Traver. 2014. Proinflammatory signaling regulates hematopoietic stem cell emergence. *Cell.* 159:1070–1085. http://dx.doi.org/10.1016/j.cell.2014.10.031

Frame, J.M., K.E. McGrath, and J. Palis. 2013. Erythro-myeloid progenitors: "definitive" hematopoiesis in the conceptus prior to the emergence of hematopoietic stem cells. *Blood Cells Mol. Dis.* 51:220–225. http://dx.doi.org/10.1016/j.bcmd.2013.09.006

Ganis, J.J., N. Hsia, E. Trompouki, J.L. de Jong, A. DiBiase, J.S. Lambert, Z. Jia, P.J. Sabo, M. Weaver, R. Sandstrom, et al. 2012. Zebrafish globin switching occurs in two developmental stages and is controlled by the LCR. *Dev. Biol.* 366:185–194. http://dx.doi.org/10.1016/j.ydbio.2012.03.021

Gekas, C., F. Dieterlen-Lièvre, S.H. Orkin, and H.K. Mikkola. 2005. The placenta is a niche for hematopoietic stem cells. *Dev. Cell.* 8:365–375. http://dx.doi.org/10.1016/j.devcel.2004.12.016

Gurskaya, N.G., V.V. Verkhusha, A.S. Shcheglov, D.B. Staroverov, T.V. Chepurnykh, A.F. Fradkov, S. Lukyanov, and K.A. Lukyanov. 2006. Engineering of a monomeric green-to-red photoactivatable fluorescent protein induced by blue light. *Nat. Biotechnol.* 24:461–465. http://dx.doi.org/10.1038/nbt1191

Haire, R.N., J.P. Rast, R.T. Litman, and G.W. Litman. 2000. Characterization of three isotypes of immunoglobulin light chains and T-cell antigen receptor alpha in zebrafish. *Immunogenetics.* 51:915–923. http://dx.doi.org/10.1007/s002510000229

Hans, S., D. Freudenreich, M. Geffarth, J. Kaslin, A. Machate, and M. Brand. 2011. Generation of a non-leaky heat shock-inducible Cre line for conditional Cre/lox strategies in zebrafish. *Dev. Dyn.* 240:108–115. http://dx.doi.org/10.1002/dvdy.22497

He, Q., C. Zhang, L. Wang, P. Zhang, D. Ma, J. Lv, and F. Liu. 2015. Inflammatory signaling regulates hematopoietic stem and progenitor cell emergence in vertebrates. *Blood.* 125:1098–1106. http://dx.doi.org/10.1182/blood-2014-09-601542

Hess, I., and T. Boehm. 2012. Intravital imaging of thymopoiesis reveals dynamic lympho-epithelial interactions. *Immunity.* 36:298–309. http://dx.doi.org/10.1016/j.immuni.2011.12.016

Isogai, S., M. Horiguchi, and B.M. Weinstein. 2001. The vascular anatomy of the developing zebrafish: an atlas of embryonic and early larval development. *Dev. Biol.* 230:278–301. http://dx.doi.org/10.1006/dbio.2000.9995

Jagannathan-Bogdan, M., and L.I. Zon. 2013. Hematopoiesis. *Development.* 140:2463–2467. http://dx.doi.org/10.1242/dev.083147

Jin, H., J. Xu, and Z. Wen. 2007. Migratory path of definitive hematopoietic stem/progenitor cells during zebrafish development. *Blood.* 109:5208–5214. http://dx.doi.org/10.1182/blood-2007-01-069005

Jin, H., R. Sood, J. Xu, F. Zhen, M.A. English, P.P. Liu, and Z. Wen. 2009. Definitive hematopoietic stem/progenitor cells manifest distinct differentiation output in the zebrafish VDA and PBI. *Development.* 136:647–654. http://dx.doi.org/10.1242/dev.029637

Jing, L., and L.I. Zon. 2011. Zebrafish as a model for normal and malignant hematopoiesis. *Dis. Model. Mech.* 4:433–438. http://dx.doi.org/10.1242/dmm.006791

Kanz, D., M. Konantz, E. Alghisi, T.E. North, and C. Lengerke. 2016. Endothelial-to-hematopoietic transition: Notch-ing vessels into blood. *Ann. N. Y. Acad. Sci.* 1370:97–108. http://dx.doi.org/10.1111/nyas.13030

Kawakami, K., A. Shima, and N. Kawakami. 2000. Identification of a functional transposase of the Tol2 element, an Ac-like element from the Japanese medaka fish, and its transposition in the zebrafish germ lineage. *Proc. Natl. Acad. Sci. USA.* 97:11403–11408. http://dx.doi.org/10.1073/pnas.97.21.11403

Kissa, K., and P. Herbomel. 2010. Blood stem cells emerge from aortic endothelium by a novel type of cell transition. *Nature.* 464:112–115. http://dx.doi.org/10.1038/nature08761

Klug, D.B., C. Carter, I.B. Gimenez-Conti, and E.R. Richie. 2002. Cutting edge: thymocyte-independent and thymocyte-dependent phases of epithelial patterning in the fetal thymus. *J. Immunol.* 169:2842–2845. http://dx.doi.org/10.4049/jimmunol.169.6.2842

Langenau, D.M., and L.I. Zon. 2005. The zebrafish: a new model of T-cell and thymic development. *Nat. Rev. Immunol.* 5:307–317. http://dx.doi.org/10.1038/nri1590

Langenau, D.M., A.A. Ferrando, D. Traver, J.L. Kutok, J.P. Hezel, J.P. Kanki, L.I. Zon, A.T. Look, and N.S. Trede. 2004. In vivo tracking of T cell development, ablation, and engraftment in transgenic zebrafish. *Proc. Natl. Acad. Sci. USA.* 101:7369–7374. http://dx.doi.org/10.1073/pnas.0402248101

Li, Z., Y. Lan, W. He, D. Chen, J. Wang, F. Zhou, Y. Wang, H. Sun, X. Chen, C. Xu, et al. 2012. Mouse embryonic head as a site for hematopoietic stem cell development. *Cell Stem Cell.* 11:663–675. http://dx.doi.org/10.1016/j.stem.2012.07.004

Lin, Y., M.C. Yoder, and M. Yoshimoto. 2014. Lymphoid progenitor emergence in the murine embryo and yolk sac precedes stem cell detection. *Stem Cells Dev.* 23:1168–1177. http://dx.doi.org/10.1089/scd.2013.0536

Medvinsky, A., and E. Dzierzak. 1996. Definitive hematopoiesis is autonomously initiated by the AGM region. *Cell.* 86:897–906. http://dx.doi.org/10.1016/S0092-8674(00)80165-8

Meeker, N.D., A.C. Smith, J.K. Frazer, D.F. Bradley, L.A. Rudner, C. Love, and N.S. Trede. 2010. Characterization of the zebrafish T cell receptor beta locus. *Immunogenetics.* 62:23–29. http://dx.doi.org/10.1007/s00251-009-0407-6

Michaëlsson, J., J.E. Mold, J.M. McCune, and D.F. Nixon. 2006. Regulation of T cell responses in the developing human fetus. *J. Immunol.* 176:5741–5748. http://dx.doi.org/10.4049/jimmunol.176.10.5741

Mitra, S., A. Alnabulsi, C.J. Secombes, and S. Bird. 2010. Identification and characterization of the transcription factors involved in T-cell development, t-bet, stat6 and foxp3, within the zebrafish, *Danio rerio. FEBS J.* 277:128–147. http://dx.doi.org/10.1111/j.1742-4658.2009.07460.x

Mold, J.E., J. Michaëlsson, T.D. Burt, M.O. Muench, K.P. Beckerman, M.P. Busch, T.H. Lee, D.F. Nixon, and J.M. McCune. 2008. Maternal alloantigens promote the development of tolerogenic fetal regulatory T cells in utero. *Science.* 322:1562–1565. http://dx.doi.org/10.1126/science.1164511

Mold, J.E., S. Venkatasubrahmanyam, T.D. Burt, J. Michaëlsson, J.M. Rivera, S.A. Galkina, K. Weinberg, C.A. Stoddart, and J.M. McCune. 2010. Fetal and adult hematopoietic stem cells give rise to distinct T cell lineages in humans. *Science.* 330:1695–1699. http://dx.doi.org/10.1126/science.1196509

Monteiro, R., P. Pinheiro, N. Joseph, T. Peterkin, J. Koth, E. Repapi, F. Bonkhofer, A. Kirmizitas, and R. Patient. 2016. Transforming growth factor β drives hemogenic endothelium programming and the transition to hematopoietic stem cells. *Dev. Cell.* 38:358–370. http://dx.doi.org/10.1016/j.devcel.2016.06.024

Mosimann, C., C.K. Kaufman, P. Li, E.K. Pugach, O.J. Tamplin, and L.I. Zon. 2011. Ubiquitous transgene expression and Cre-based recombination driven by the ubiquitin promoter in zebrafish. *Development.* 138:169–177. http://dx.doi.org/10.1242/dev.059345

Müller, A.M., A. Medvinsky, J. Strouboulis, F. Grosveld, and E. Dzierzak. 1994. Development of hematopoietic stem cell activity in the mouse embryo. *Immunity.* 1:291–301. http://dx.doi.org/10.1016/1074-7613(94)90081-7

Murayama, E., K. Kissa, A. Zapata, E. Mordelet, V. Briolat, H.F. Lin, R.I. Handin, and P. Herbomel. 2006. Tracing hematopoietic precursor migration to successive hematopoietic organs during zebrafish development. *Immunity.* 25:963–975. http://dx.doi.org/10.1016/j.immuni.2006.10.015

Nishikawa, S.I., S. Nishikawa, H. Kawamoto, H. Yoshida, M. Kizumoto, H. Kataoka, and Y. Katsura. 1998. In vitro generation of lymphohematopoietic cells from endothelial cells purified from murine embryos. *Immunity.* 8:761–769. http://dx.doi.org/10.1016/S1074-7613(00)80581-6

North, T.E., W. Goessling, M. Peeters, P. Li, C. Ceol, A.M. Lord, G.J. Weber, J. Harris, C.C. Cutting, P. Huang, et al. 2009. Hematopoietic stem cell development is dependent on blood flow. *Cell.* 137:736–748. http://dx.doi.org/10.1016/j.cell.2009.04.023

Ottersbach, K., and E. Dzierzak. 2005. The murine placenta contains hematopoietic stem cells within the vascular labyrinth region. *Dev. Cell.* 8:377–387. http://dx.doi.org/10.1016/j.devcel.2005.02.001

Owen, J., J. Punt, S. Stranford, and P. Jones. 2013. Kuby Immunology. Seventh edition. W.H. Freeman, New York.

Palis, J., and M.C. Yoder. 2001. Yolk-sac hematopoiesis: the first blood cells of mouse and man. *Exp. Hematol.* 29:927–936. http://dx.doi.org/10.1016/S0301-472X(01)00669-5

Palis, J., S. Robertson, M. Kennedy, C. Wall, and G. Keller. 1999. Development of erythroid and myeloid progenitors in the yolk sac and embryo proper of the mouse. *Development.* 126:5073–5084.

Pancer, Z., and M.D. Cooper. 2006. The evolution of adaptive immunity. *Annu. Rev. Immunol.* 24:497–518. http://dx.doi.org/10.1146/annurev.immunol.24.021605.090542

Picelli, S., A.K. Björklund, O.R. Faridani, S. Sagasser, G. Winberg, and R. Sandberg. 2013. Smart-seq2 for sensitive full-length transcriptome profiling in single cells. *Nat. Methods.* 10:1096–1098. http://dx.doi.org/10.1038/nmeth.2639

Picelli, S., O.R. Faridani, A.K. Björklund, G. Winberg, S. Sagasser, and R. Sandberg. 2014. Full-length RNA-seq from single cells using Smart-seq2. *Nat. Protoc.* 9:171–181. http://dx.doi.org/10.1038/nprot.2014.006

Schorpp, M., M. Bialecki, D. Diekhoff, B. Walderich, J. Odenthal, H.M. Maischein, A.G. Zapata, and T. Boehm. 2006. Conserved functions of Ikaros in vertebrate lymphocyte development: genetic evidence for distinct larval and adult phases of T cell development and two lineages

of B cells in zebrafish. *J. Immunol.* 177:2463–2476. http://dx.doi.org/10.4049/jimmunol.177.4.2463

Seelye, S.L., P.L. Chen, T.C. Deiss, and M.F. Criscitiello. 2016. Genomic organization of the zebrafish (*Danio rerio*) T cell receptor alpha/delta locus and analysis of expressed products. *Immunogenetics.* 68:365–379. http://dx.doi.org/10.1007/s00251-016-0904-3

Somamoto, T., Y. Yoshiura, T. Nakanishi, and M. Ototake. 2005. Molecular cloning and characterization of two types of CD8alpha from ginbuna crucian carp, *Carassius auratus langsdorfii. Dev. Comp. Immunol.* 29:693–702. http://dx.doi.org/10.1016/j.dci.2004.11.006

Sood, R., and P. Liu. 2012. Novel insights into the genetic controls of primitive and definitive hematopoiesis from zebrafish models. *Adv. Hematol.* 2012:830703. http://dx.doi.org/10.1155/2012/830703

Sood, R., M.A. English, C.L. Belele, H. Jin, K. Bishop, R. Haskins, M.C. McKinney, J. Chahal, B.M. Weinstein, Z. Wen, and P.P. Liu. 2010. Development of multilineage adult hematopoiesis in the zebrafish with a runx1 truncation mutation. *Blood.* 115:2806–2809. http://dx.doi.org/10.1182/blood-2009-08-236729

Stachura, D.L., and D. Traver. 2011. Cellular dissection of zebrafish hematopoiesis. *Methods Cell Biol.* 101:75–110. http://dx.doi.org/10.1016/B978-0-12-387036-0.00004-9

Stachura, D.L., and D. Traver. 2016. Cellular dissection of zebrafish hematopoiesis. *Methods Cell Biol.* 133:11–53. http://dx.doi.org/10.1016/bs.mcb.2016.03.022

Takizawa, F., K. Araki, K. Ito, T. Moritomo, and T. Nakanishi. 2007. Expression analysis of two Eomesodermin homologues in zebrafish lymphoid tissues and cells. *Mol. Immunol.* 44:2324–2331. http://dx.doi.org/10.1016/j.molimm.2006.11.018

Tamplin, O.J., E.M. Durand, L.A. Carr, S.J. Childs, E.J. Hagedorn, P. Li, A.D. Yzaguirre, N.A. Speck, and L.I. Zon. 2015. Hematopoietic stem cell arrival triggers dynamic remodeling of the perivascular niche. *Cell.* 160:241–252. http://dx.doi.org/10.1016/j.cell.2014.12.032

Thisse, C., and B. Thisse. 2008. High-resolution in situ hybridization to whole-mount zebrafish embryos. *Nat. Protoc.* 3:59–69. http://dx.doi.org/10.1038/nprot.2007.514

Wendl, T., K. Lun, M. Mione, J. Favor, M. Brand, S.W. Wilson, and K.B. Rohr. 2002. Pax2.1 is required for the development of thyroid follicles in zebrafish. *Development.* 129:3751–3760.

Westerfield, M. 2000. The Zebrafish Book: A Guide for the Laboratory Use of Zebrafish (*Danio rerio*). University of Oregon Press, Eugene, OR.

Xu, J., L. Zhu, S. He, Y. Wu, W. Jin, T. Yu, J.Y. Qu, and Z. Wen. 2015. Temporal-spatial resolution fate mapping reveals distinct origins for embryonic and adult microglia in zebrafish. *Dev. Cell.* 34:632–641. http://dx.doi.org/10.1016/j.devcel.2015.08.018

Xu, J., T. Wang, Y. Wu, W. Jin, and Z. Wen. 2016. Microglia colonization of developing zebrafish midbrain is promoted by apoptotic neuron and lysophosphatidylcholine. *Dev. Cell.* 38:214–222. http://dx.doi.org/10.1016/j.devcel.2016.06.018

Yoder, J.A., T.M. Orcutt, D. Traver, and G.W. Litman. 2007. Structural characteristics of zebrafish orthologs of adaptor molecules that associate with transmembrane immune receptors. *Gene.* 401:154–164. http://dx.doi.org/10.1016/j.gene.2007.07.014

Yokota, T., J. Huang, M. Tavian, Y. Nagai, J. Hirose, J.C. Zúñiga-Pflücker, B. Péault, and P.W. Kincade. 2006. Tracing the first waves of lymphopoiesis in mice. *Development.* 133:2041–2051. http://dx.doi.org/10.1242/dev.02349

Yoon, S., S. Mitra, C. Wyse, A. Alnabulsi, J. Zou, E.M. Weerdenburg, A.M. van der Sar, D. Wang, C.J. Secombes, and S. Bird. 2015. First demonstration of antigen induced cytokine expression by CD4-1+ lymphocytes in a poikilotherm: studies in zebrafish (*Danio rerio*). *PLoS One.* 10:e0126378. http://dx.doi.org/10.1371/journal.pone.0126378

Yoshimoto, M., P. Porayette, N.L. Glosson, S.J. Conway, N. Carlesso, A.A. Cardoso, M.H. Kaplan, and M.C. Yoder. 2012. Autonomous murine T-cell progenitor production in the extra-embryonic yolk sac before HSC emergence. *Blood.* 119:5706–5714. http://dx.doi.org/10.1182/blood-2011-12-397489